# Application of Wavelet Transform for Determining Diagnostic Signs

Volodymyr Eremenko[1[0000-0002-4330-7518]], Artur Zaporozhets[2[0000-0002-0704-4116]], Volodymyr Isaenko[3[0000-0001-8010-8844]], Kateryna Babikova[3[0000-0002-5053-1999]]

[1] National Technical University of Ukraine "Igor Sikorsky Kyiv Polytechnical Institute", Kyiv, Ukraine
[2] Institute of Engineering Thermophysics of NAS of Ukraine, Kyiv, Ukraine
[3] National Aviation University, Kyiv, Ukraine
a.o.zaporozhets@nas.gov.ua

**Abstract.** It is proposed to apply the wavelet transform to localize in time the frequency components of the information signals in this article. The wavelet transform allows to fulfil time-frequency analysis of signals, which is very important for studying the structure of a composite material from the mode composition of free oscillations. The proposed approach to the development of information signals using wavelet transform makes it possible to further study the nature of the occurrence of free oscillations and the propagation of acoustic waves in individual layers of composites and to study the change in the structure of composites from the changes in the three-dimensional wavelet spectrum.

**Keywords:** wavelet transform, MHAT wavelet, Morlet wavelet, diagnostic signs, information signal, composite material, free oscillation method

## 1 Introduction

Information signals obtained in the process of diagnosing composite materials by low-frequency acoustic methods belong to the class of single-pulse signals with locally concentrated features. These are, for example, signals of free oscillations, whose modes have not only frequency, but also temporal distribution, signals of impulse impedance method change frequency and current carrier phase for one radio pulse, signals of low-speed impact method locally change their shape depending on material defectiveness.

For such signals, the task of identifying diagnostic signs is significantly more difficult than for signals in which the information component is evenly distributed over the observation interval [1, 2]. This is explained by the fact that diagnostic signs are focused on small time intervals or fragments of signal realization, and the signal itself has a rather complex form that cannot be described by a formal constructive model. The most common methods for isolating diagnostic features of such signals are [3, 4, 5, 6]:

- methods for evaluating the integral characteristics – the center of mass of the pulse, the similarity coefficients, etc. These methods have high noise immunity, but have very little sensitivity to local changes in signal parameters;

- methods of decomposition of signals with an orthogonal basis. In general, they provide information about the shape of the pulsed signal, but provide only an integral representation of its components throughout the entire domain of definition and are not sensitive to local variations in characteristics;
- methods of structural analysis using signal segmentation as a sequence of separate fragments. Based on segmentation signal clustering is performed, chains of clusters are used to structure the signal;
- methods for representing signals in phase space –space, which is determined by a finite set of state parameters. The disadvantage is the need for multiple repetition of the pulse signal and the analysis of multidimensional data arrays;
- heuristic methods, in particular, methods using neural network technologies, which allow to select informative fragments of signals and to make a comparison with the "reference" ones.

Classical methods for processing signals of low-frequency acoustic diagnostic methods, in particular, the method of decomposing signals with an orthogonal basis (generalized Fourier transform), which give an integral representation of the signal components in the entire domain of their definition, are ineffective [7]. Therefore it was proposed to apply the wavelet transform for localizing the frequency components of information signals in time [8].

The signals of free oscillations are damped and consist of several modes, then each mode, depending on which layer of the composite it is excited, will have its own amplitude, frequency and attenuation coefficient. That is, knowing the time behavior of each mode, one can draw conclusions about the structure of the controlled zone of the composite [9]. The continuous wavelet transform allows to carry out a time-frequency analysis [10]. These studies can be used in many areas, including the monitoring of complex technical systems [11, 12].

## 2 Main Part

The wavelet transform combines two types of transformations – direct and inverse, which, respectively, translate the studied function *f(t)* into a set of $W_\psi(a,b)f$ wavelet coefficients and vice versa [13]. The direct wavelet transform is performed according to the rule:

$$W_\psi(a,b)f = \frac{1}{\sqrt{C_\psi}} \int_{-\infty}^{\infty} \frac{1}{\sqrt{|a|}} \psi^* \left( \frac{x-b}{a} \right) f(t)dt , \qquad (1)$$

where *a* and *b* are the parameters that determine, respectively, the scale and offset of the function $\psi$, which is called the analyzing wavelet; $C_\psi$ is normalization coefficient.

The basic, or maternal, wavelet $\psi$ forms with the help of stretch marks and landslides a family of functions $\psi\ (t–b/a)$. Having a known set of coefficients $W_\psi(a, b)f$, we can restore the original form of the function *f(t)*:

$$f(t) = \frac{1}{\sqrt{C_\psi}} \int_{-\infty}^{\infty} \int_{-\infty}^{\infty} \frac{1}{\sqrt{|a|}} \psi\left(\frac{t-b}{a}\right) \left[W_\psi(a,b) f\right] \frac{da \cdot db}{a^2}. \quad (2)$$

The direct (1) and the inverse (2) transforms depend on some function $\psi(t) \in L^2(R)$ which is called the basic wavelet. In practice, the only restriction on its choice is the condition for the finiteness of the normalizing coefficient [14]:

$$C_\psi = \int_{-\infty}^{\infty} \frac{|\hat{\psi}(\omega)|}{|\omega|} d\omega = 2\int_0^{\infty} \frac{|\hat{\psi}(\omega)|^2}{|\omega|} d\omega < \infty, \quad (3)$$

where $\hat{\psi}(\omega)$ is Fourier image of the $\psi(\omega)$ wavelet:

$$\hat{\psi}(\omega) = \frac{1}{\sqrt{2\pi}} \int_{-\infty}^{\infty} \psi(t) e^{-i\omega t} dt. \quad (4)$$

This condition satisfies many functions, so it is possible to choose the type of wavelet that is most suitable for solving a specific problem. In particular, for analyzing damped harmonic oscillations, it is more expedient to select wavelets, which are also damped oscillations. The article deals with the MHAT-wavelet and Morlet wavelet.

The condition (3) means that the Fourier transform of the wavelet is zero at zero frequency, i.e. $\hat{\psi}(\omega)\big|_{\omega=0} = 0$. In another case the denominator of the fraction in the integral (3) is equal to zero, while the numerator has a nonzero value, and the $C_\psi$ coefficient ceases to be finite.

In turn, this requirement can be presented in another form. Since the Fourier transform $\hat{\psi}(\omega)$ at zero frequency has the form $\int_{-\infty}^{\infty} \psi(t) dt$, it can write the following:

$$\hat{\psi}(\omega) = \frac{1}{\sqrt{2\pi}} \int_{-\infty}^{\infty} \psi(t) e^{-i\omega t} dt. \quad (5)$$

A characteristic feature of the analyzing wavelets is time-frequency localization. This means that wavelets $\psi(t)$ and their Fourier transforms $\hat{\psi}(\omega)$ differ significantly from zero only at small time intervals and frequencies, and differ very little from zero (or simply equal to zero) outside these intervals.

The quantitative measure of the localization of a function $\psi(t) \in L^2(\mathbf{R})$ can be its center $\langle t \rangle$ and radius $\Delta_t^2$:

$$\langle t \rangle = \frac{1}{\|\psi\|^2} \int_{-\infty}^{\infty} t |\psi(t)|^2 dt, \quad (6)$$

$$\Delta_t^2 = \frac{1}{\|\psi\|^2} \int_{-\infty}^{\infty} \left[t - \langle t \rangle\right]^2 |\psi(t)|^2 \, dt. \tag{7}$$

In this case, the effective wavelet width is assumed to be $2\Delta_t$.

Nowadays a large number of basic wavelet functions are known [15, 16]. As mentioned above, the members of any family of wavelets must satisfy condition (7) one of such families, the Gauss and wavelets. The functions of this family are derived from the Gaussian exponent:

$$g_n(t) = (-1)^{n+1} \frac{d^n}{dt^t} e^{-t^2/2}, \; n \in \mathbf{N}. \tag{8}$$

The normalization coefficient takes the value

$$C_{g_n} = 2\pi(n-1)!, \; 0 < n < \infty. \tag{9}$$

The most widely used Gaussian wavelets of small orders. The properties of Gaussian wavelets are discussed in detail in [17].

### 2.1 MHAT Wavelet

This wavelet is a second-order wavelet of the family of Gaussian wavelets (Fig. 1) and is formed by a double differentiation of the Gauss function:

$$g_2(t) = (1-t^2)e^{-t^2/2}. \tag{10}$$

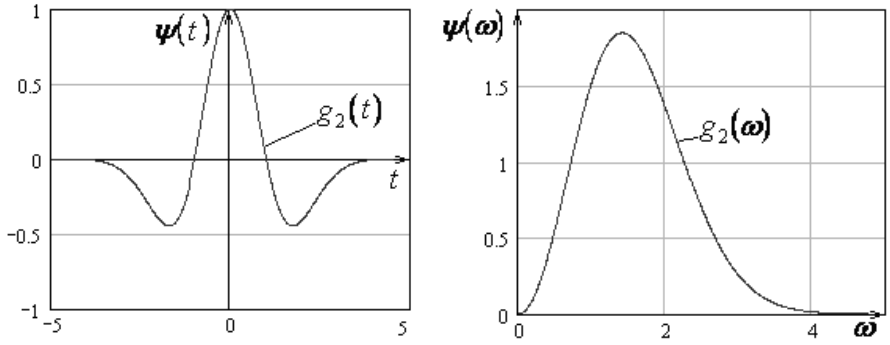


(a) (b)

**Fig. 1.** Second order Gaussian wavelet (MHAT) (a) and its Fourier transform (b)

The Fourier transform of this wavelet is

$$\hat{\psi}(\omega) = \sqrt{2\pi}\omega^2 e^{-\omega^2/2}. \tag{11}$$

The graph of this function is shown in Fig. 1 (b). MHAT wavelets are well localized in both the time and frequency domains. The centers and localization radii in both areas have the following meanings; $\langle t \rangle = 0$ ; $\Delta_t = 1.08$, $\langle \omega \rangle = 1.51$, $\Delta_\omega = 0.49$.

### 2.2 Morlet Wavelet

The analytical representation of the Morlet wavelet and its Fourier transform is given by the following expressions:

$$\psi(t) = e^{-t^2/\alpha^2} \left[ e^{ik_0 t} - e^{-k_0^2 \alpha^2/4} \right], \tag{12}$$

$$\hat{\psi}(\omega) = \alpha\sqrt{\pi} \left[ e^{-\alpha^2 (k_0 - \omega)^2/4} - e^{-\alpha^2 (k_0 + \omega)^2/4} \right]. \tag{13}$$

The Morlet wavelet is a plane wave modulated by a Gausian. The parameter α specifies the width of the Gausian, the parameter $k_0$ is the frequency of the plane wave. Usually it choose $\alpha^2 = 2$ and $k_0 = 2\pi$. With these values with sufficient accuracy it can be taken [18]:

$$\psi(t) = e^{-t^2/\alpha^2} e^{i2\pi t}, \tag{14}$$

$$\hat{\psi}(\omega) = \alpha\sqrt{\pi} e^{-\alpha^2 (2\pi - \omega)^2/4}. \tag{15}$$

Graphs of these functions are shown in Fig. 2.

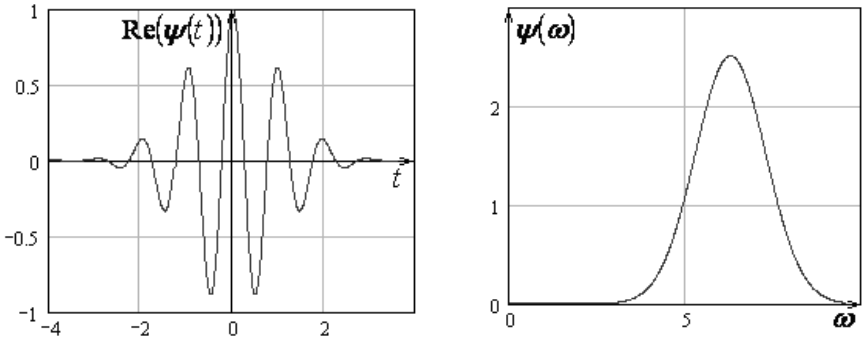


(a) (b)

**Fig. 2.** The real part of the Morlet wavelet (a) and its Fourier transform (b)

The center and localization radius of the Morlet wavelet in the time domain are determined by the corresponding values; $\langle t \rangle = 0$, $\Delta_t = \alpha/2$. In the Morlet wavelet, only zero moment is equal zero.

The definitions of the integral wavelet transform introduced above cannot be used in practice, since in digital processing of results the main transformation objects are not functions defined on the entire time axis, but discrete signals whose length are always finite [19]. For this reason, instead of the above theoretical concepts, their practical counterparts (assessments) should be introduced.

We assume that the signal is given by the function values with a constant step $\Delta t$:

$$f_k = f\left(t_k\right),\ t_k = \Delta t \cdot k,\ k = \overline{0, N-1}. \tag{16}$$

To estimate the wavelet transform of this sequence, we use the following expression:

$$W(a,b) = \frac{1}{n(a,b)} \sum_{k=0}^{N-1} f_k \psi^* \left( \frac{t_k - b}{a} \right), \tag{17}$$

$$n(a,b) = \sum_{k=0}^{N-1} e^{-\frac{1}{B}\left(\frac{t_k - b}{a}\right)^2}. \tag{18}$$

where $B$=2 for MHAT wavelet and $B=\alpha^2$ for Morlet wavelet

In the transition from (1) to (17), the multiplier $\sqrt{a}$ from the denominator of the formula (1) is replaced as follows

$$\int_{-\infty}^{\infty} e^{-\frac{(t-b)^2}{a^2 B}} dt = a\sqrt{B\pi}, \tag{19}$$

the discrete approximation of which is function (18).

This made it possible to eliminate the dependence of the amplitudes of the harmonic components on the parameter $a$, which usually makes it difficult to correctly estimate their relative intensities from the graphic image of the wavelet spectra. In addition, the function $n(a,b)$ as an approximation allows to "equalize" for different values of the scale factor $a$ the number of samples of the original function involved in the calculation [20].

Calculating the wavelet transform in the scale-offset coordinates is somewhat inconvenient for perception, since the scale $a_i$ specified with constant pitch compresses the high-frequency region and the components of the signal under study that belong to this region become difficult to distinguish. Therefore, it is proposed by replacing $\nu_i = 1/a_i$ to switch to $\nu_i$ value that is analogous to the frequency in the Fourier transform [21]. Then a pair of wavelet transforms of the function $f(t)$ with (17) will look like this:

$$W_\psi(\nu,b) f = \frac{1}{n(\nu,b)} \int \psi^* \left((t-b)\nu\right) f(t) dt, \tag{20}$$

$$f(t)=\frac{-\sqrt{B\pi}}{C_\psi}\int\int\psi\left((t-b)\nu\right)\left[W_\psi(\nu,b)\,f\right]d\nu\cdot db\,, \tag{21}$$

where $n(\nu,b)=\int_{-\infty}^{\infty}e^{-\frac{(t-b)^2\nu^2}{B}}dt$.

The amplitude value of the discrete signal wavelet function will be calculated by the following equations:

$$W(\nu_i,b_j)=\frac{1}{n(\nu_i,b_j)}\sum_{k=0}^{N-1}f_k\psi^*\left((t_k-b_j)\nu_i\right), \tag{22}$$

$$n(\nu_i,b_j)=\sum_{k=0}^{N-1}e^{-\frac{1}{B}\left((t_k-b_j)\nu_i\right)^2}\,. \tag{23}$$

### 2.3 Discretization of Arguments

Each wavelet has its own shape and characteristic size, which for a fixed value of the scale factor is determined by the value

$$d_a=2\Delta_t a\,, \tag{24}$$

where $\Delta_t$ is the wavelet radius.

The function $W(a,b)$ (22) determines the correlation between the analyzing wavelet located at a point $b$ and at a certain part of a signal of $d_a$ length with a center at a point $b$. The module of this function takes the greatest value in the case when the size of the wavelet coincides with the size of the "current" signal detail. In the case of polyharmonic functions, the natural measure of the scale of its details is the period of the harmonic components, while the measure of the wavelet length $d_a$ is determined by the value $a$ of the scale factor.

For a polyharmonic function defined on a grid with a step $\Delta t=const$, the range of periods of harmonics is determined by the quantities $P_{\min}=2\Delta_t$, $P_{\max}=(N-1)\Delta_t$. In accordance with this, the largest and smallest values of the scale factor are selected from the condition of matching the size of the wavelet and the limiting periods of harmonious components

$$2\Delta_t a_{\min}=P_{\min}\,,\ 2\Delta_t a_{\max}=P_{\max}\,, \tag{25}$$

where we get

$$a_{\min}=\Delta t/\Delta_t\,,\ a_{\max}=(N-1)\Delta t/2\Delta_t\,. \tag{26}$$

Note that these values are taken in cases where it is necessary to perform a signal analysis in the full scale range. Often, however, it is advisable to examine the signal in a narrower range of scales. In this case, the value $a_{\min}$ and $a_{\max}$ choose from other considerations.

We propose a discretization step $\Delta a = \frac{a_{\max} - a_{\min}}{Na - 1}$ of the scales, after which we define the discrete values of the scale factors $a_i = a_{\min} + \Delta a \cdot i$.

Since the width of the spectral line increases with increasing scale, sometimes the value of the parameter is presented on a logarithmic scale.

If the calculation of the wavelet transform is carried out according to (22), (23), then the minimum and maximum value of the quantity ν can be calculated using equations (25). Values $\nu_i$ are calculated with a constant step $\Delta\nu = \frac{\nu_{\max} - \nu_{\min}}{Na - 1}$ by the formula $\nu_i = \nu_{\min} + \Delta\nu \cdot i$.

In the simplest case, the boundaries of the landslide range are defined as follows $b_{\min} \geq 0$, $b_{\max} \leq (N-1)\Delta t$, and discrete values of the displacements can be calculated by the following formulas:

$$b_j = b_{\min} + \Delta b \cdot j, \tag{27}$$

$$\Delta b = \frac{b_{\max} - b_{\min}}{Nb - 1}. \tag{28}$$

With this method of discretization of the parameter $b$ near the boundaries $b_{min}$ and $b_{max}$ of magnitude $W(a_i,b_j)$ will be calculated with errors, since it is impossible to use the entire length of the analyzing wavelet near the boundaries. To exclude marginal effects, it is necessary to calculate the wavelet transform only for landslide values that are remote from the boundaries by an amount equal to the current radius of the wavelet $a\Delta_t$. With this approach, formula (26) is transformed as follows

$$b_j = b_{\min} + \Delta b \cdot j, \quad j = J_a^* + 1, ..., Nb - J_a^* - 1, \tag{29}$$

where $J_a^*$ is the radius of the wavelet, expressed in units $\Delta b$, which corresponds to the current scale value $a$ (for the Morlet wavelet)

$$J_a^* = \left[ \frac{a_i \alpha}{2\Delta b} \right]. \tag{30}$$

In the case of application instead of the scale of the formula we get:

$$J_\nu^* = \left[ \frac{\alpha}{2\Delta b \nu_i} \right]. \tag{31}$$

In these formulas, the rounding operation to the nearest integer is indicated by square brackets.

The set of nodes of the discrete grid, which is defined by formulas (25) and (29), is called the probability triangle. Note that very often the edge effects are ignored, and the results of the wavelet analysis are simply represented in the rectangular area of the nodes (25) and (27).

### 2.4 Construction of a Plurality of Diagnostic Features

The selection of each individual mode of oscillation is an important step in the study of the properties and nature of the destruction of composite materials. Attenuation of the components of free oscillations carries information about the quality factor of the controlled zone of the composite. This allows to investigate defects that are not associated with delamination, such as fatigue and impact damage to the surface.

The proposed approach with the use of wavelet transform makes it possible to further study the nature of the propagation of acoustic waves in individual layers of composites and to investigate the change in the structure of composites by the revealed changes in the wavelet spectrum of free vibrations.

Next we consider the wavelet transform of signals received in the intact and damaged area of a cellular panel with a thickness of 20 mm. The amplitude spectra of these signals are shown in Fig. 3, 4.

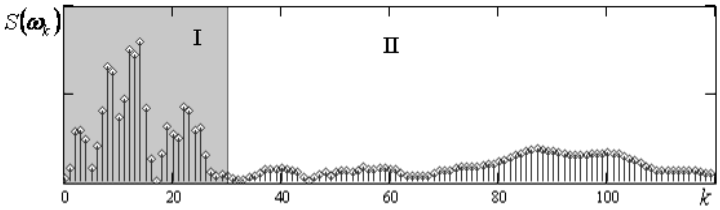


**Fig. 3.** Amplitude spectrum of the signal of free oscillations of the intact area of the cellular panel

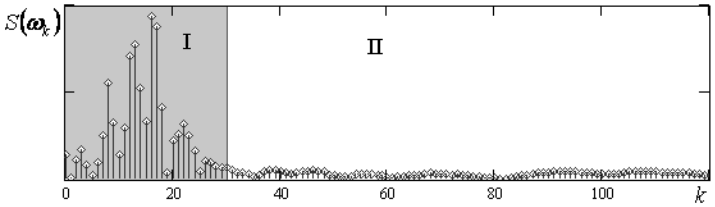


**Fig. 4.** Amplitude spectrum of a signal of free oscillations of a zone with a defect of 20 mm radius of a cellular panel

The estimated amplitude spectra preliminarily determine the frequency range within which the wavelet transform will be performed — zone I in Fig. 3, 4.

Fig. 5 shows plots of the amplitude wavelet spectra of these signals, calculated by a Morlet wavelet in the selected frequency range.

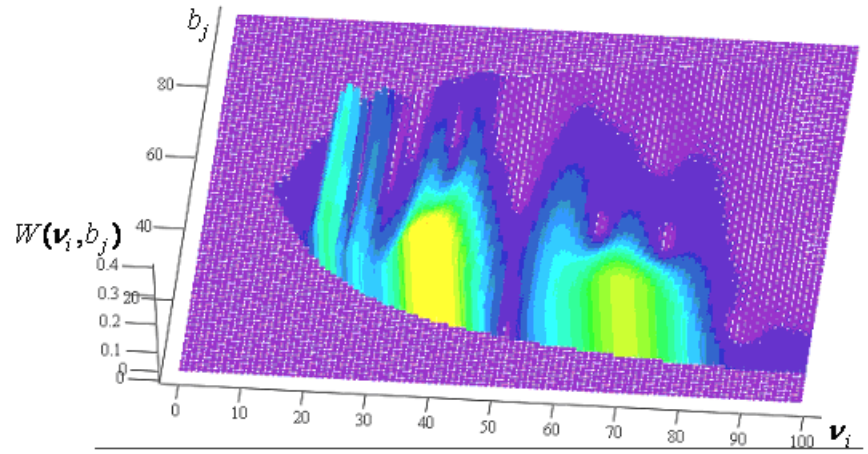


(a)

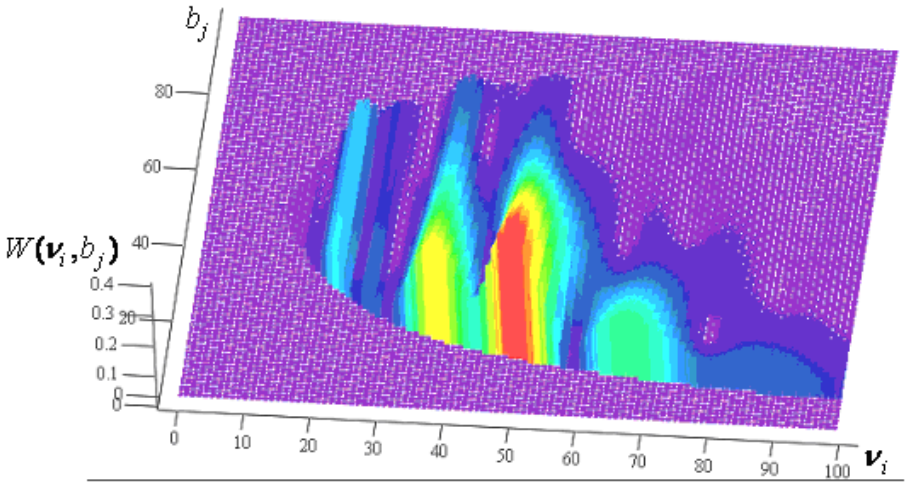


(b)

**Fig. 5.** Graphs of amplitude wavelet functions of signals of free oscillations: a – intact zone, b – zone with damage of 20 mm radius

From these figures it can be seen that, for example, the 1st, 2nd and 3rd modes of oscillations change the nature of the attenuation with the appearance of a defect. In fig. 6 shows the restored third mode oscillations of the benign zone and the damaged zone. Its attenuation coefficient changes with the appearance of a defect from 4.72 to 2.56.

For faster decision making on the presence or absence of a defect in the controlled area of a composite material, it is proposed to compare the amplitude wavelet spectra of free oscillations of the reference and controlled areas, calculated with the same shift. For example, in fig. 7(a) amplitude wavelet spectra of a signal of free oscillations of a benign zone with shifts $b_j = b1,\ j = 30,\ \ b_j = b2,\ j = 50,\ \ b_j = b3,\ j = 70$ are presented.

Fig. 7(b) shows similar spectra of free oscillations of a zone with a defect diameter of 20 mm. In other words, these spectra are actually a cross section of the graphs in Fig. 5.

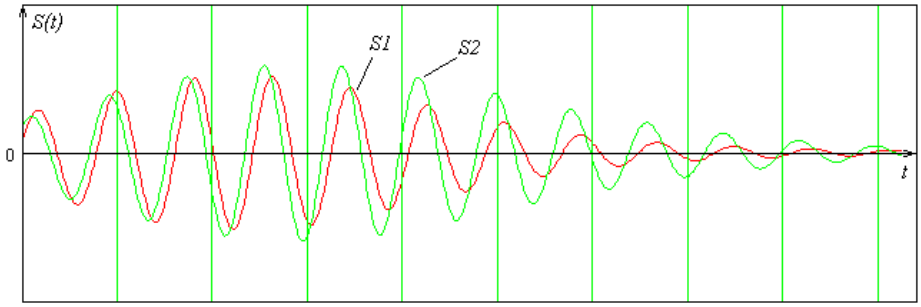


**Fig. 6.** The third damping component of free vibrations of the benign zone (S1) and the damaged zone (S2)

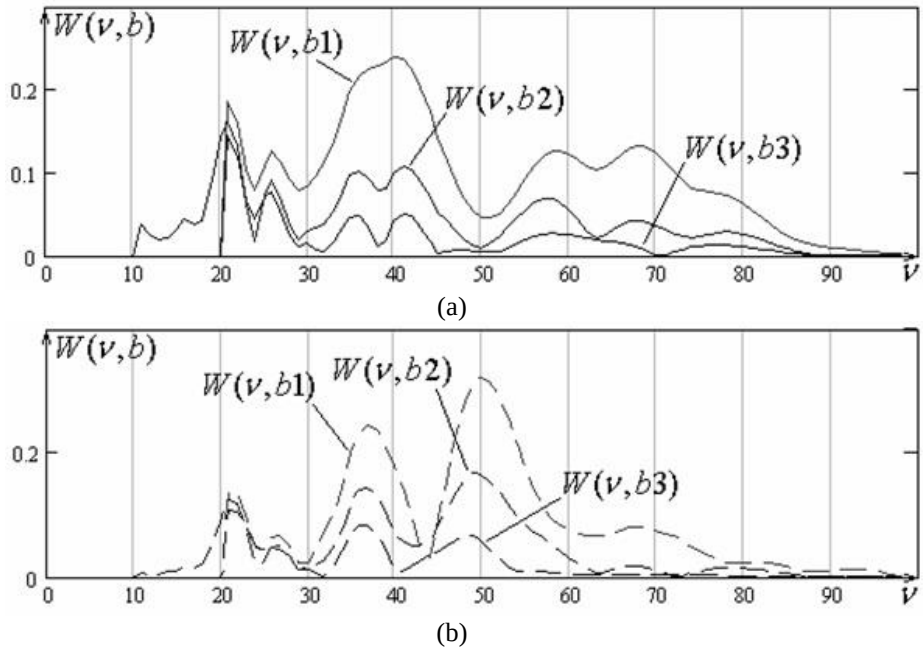


**Fig. 7.** Plots of amplitude wavelet spectra of free vibrations of the intact zone (a) and zones with a separation of 20 mm (b) at displacements b1<b2 <b3

The obtained wavelet spectra in fig. 7 are convenient for visual comparison, and also allow you to more accurately determine the frequency range of each individual mode in order to reduce errors in its recovery.

## 3 Conclusions

A constructive mathematical model of the information signal field of the process of diagnosing composite materials was constructed, which made it possible to describe the interaction of mechanical perturbation fields in composite materials with defects of various types. This allowed to use experimental results for statistical evaluation of field characteristics, to conduct a wide range of mathematical and computer model experiments.

Methods of primary processing of information signals of acoustic diagnostic methods in time-frequency coordinates have been improved and investigated, which made it possible to carry out a structural analysis of single-pulse signals and signals with locally concentrated parameter changes and to increase the probability of diagnosis by 20%.

## References


1. Zaporozhets, A., Eremenko, V., Serhiienko, R., Ivanov, S. Methods and Hardware for Dianosing Thermal Power Equipment Based on Smart Grid Technology, *Advances in Intelligent Systems and Computing III*, 2019, Vol. 871, pp. 476-492. doi: 10.1007/978-3-030-01069-0_34
2. Zaporozhets, A.A., Eremenko, V.S., Serhiienko, R.V., Ivanov, S.A. Development of an Intelligent System for Diagnosing the Technical Condition of the Heat Power Equipment. 2018 IEEE 13th International Scientific and Technical Conference on Computer Sciences and Information Technologies (CSIT), 11-14 September, 2018, Lviv, Ukraine. doi: 10.1109/STC-CSIT.2018.8526742
3. Bhattacharyya, A., Sharma, M., Pachori, R.B., Sircar, P., Acharya, U.R. A novel approach for automated detection of focal EEG signals using empirical wavelet transform. Neural Computing and Applications, 2018, Vol. 29, Issue 8, pp. 47-57. doi: 10.1007/s00521-016-2646-4
4. Xiong, L., Xu, Z., Shi, Y.-Q. An integer wavelet transform based scheme for reversible data hiding in encrypted images. Multidimensional Systems and Signal Processing, 2018, Vol. 29, Issue 3, pp. 1191-1202. doi: 10.1007/s11045-017-0497-5
5. Topalov, A., Kondratenko, Y., Kozlov, O. Computerized Intelligent System for Remote Diagnostics of Level Sensors in the Floating Dock Ballast Complexes. *CEUR Workshop Proceedings*, Vol. 2105, 2018. Online: http://ceur-ws.org/Vol-2105/10000094.pdf
6. Shtovba, S., Pankevych, O. Fuzzy Technology-Based Cause Detection of Structural Cracks of Stone Buildings. *CEUR Workshop Proceedings*, Vol. 2105, 2018. Online: http://ceur-ws.org/Vol-2105/10000209.pdf
7. Pavlov, A.N., Anishchenko, V.S. Multifractal analysis of complex signals. *Physics-Uspekhi*, 2007, Vol. 50, Issue 8, pp. 819. doi: 10.1070/PU2007v050n08ABEH006116
8. Eremenko, V., Zaporozhets, A., Sverdlova, A. Application Hilbert transform in diagnosis using the impedance method. IEEE 39th International Conference on Electronics and Nanotechnology (ELNANO), 16-18 April 2019, Kyiv, Ukraine.
9. Zaporozhets, A.O., Redko, O.O., Babak, V.P., Eremenko, V.S., Mokiychuk, V.M. Method of indirect measurement of oxygen concentration in the air. *Scientific Bulletin of National Mining University*, 2018, №5, pp. 105-144. doi: 10.29202/nvngu/2018-5/14

10. Lee, T.-Y.,Shen, H.-W. Efficient Local Statistical Analysis via Integral Histograms with Discrete Wavelet Transform. *IEEE Tranactions on Visualization and Computer Graphics*, 2013, Vol. 19, Issue 2, pp. 2693-2702, doi: 10.1109/TVCG.2013.152
11. Popov, O., IatsyshynA., Kovach, V., Artemchuk, V., Taraduda, D., Sobyna, V., Sokolov, D., Dement, M., Yatsyshyn, T., Matvieieva, I. Analysis of Possible Causes of NPP Emergencies to Minimize Risk of Their Occurrence. *Nuclear and Radiation Safety*, 2019, Vol. 81, Issue 1, pp. 75-80. doi: 10.32918/nrs.2019.1(81).13
12. Popov, O., IatsyshynA., Kovach, V., Artemchuk, V., Taraduda, D., Sobyna, V., Sokolov, D., Dement, M., Yatsyshyn, T. Conceptual Approaches for Development of Informational and Analytical Expert System for Assessing the NPP impact on the Environment. *Nuclear and Radiation Safety*, Vol. 79, Issue 3, pp. 56-65. doi: 10.32918/nrs.2018.3(79).09
13. Strickland, R.N., Hahn, H. Wavelet transform methods for object detection and recovery. *IEEE Transactions on Image Processing*, 1997, Vol. 6, Issue 5, pp. 724-735, doi: 10.1109/83.568929
14. Babak., V., Mokiychuk, V., Zaporozhets, A., Redko, O. Improving the efficiency of fuel combustion with regard to the uncertainty of measuring oxygen concentration. *Eastern-European Journal of Enterprise Technologies*, 2016, Vol. 6, №8, pp. 54-59. doi: 10.15587/1729-4061.2016.85408
15. Plett, M.I. Transient Detection With Cross Wavelet Transforms and Wavelet Coherence. *IEEE Transactions on Signal Processing*, 2007, Vol. 55, Issue 5, pp. 1605-1611, doi: 10.1109/TSP.2006.890874
16. Li, H. Complex Morlet wavelet amplitude and phase map based bearing fault diagnosis. 2010 8th World Congress on Intelligent Control and Automation, 7-9 July 2010, Jinan, China. doi: 10.1109/WCICA.2010.5554232
17. Babak, S., Babak, V., Zaporozhets, A., Sverdlova, A. Method of Statistical Spline Functions for Solving Problems of Data Approximation and Prediction of Objects State. *CEUR Workshop Proceedings*, Vol. 2353, 2019. Online: http://ceur-ws.org/Vol-2353/paper64.pdf
18. Kumawat, P.N., Verma, D.K., Zaveri, N. Comparison between Wavelet Packet Transform and M-band Wavelet Packet Transform for Identification of Power Quality Disturbances. *Power Research*, 2018, Vol. 14, Issue 1, pp. 37-45. doi: 10.33686/pwj.v14i1.142183
19. Xia, F., Ruan, Y., Yu, Y., Guo, Q., Xi, J., Tong, J. Retrieve the Material Related Parameters from a Self-Mixing Signal Using Wavelet Transform. IEEE International Frequency Control Symposium (IFCS), 21-24 May 2018, Olympic Valley, CA, USA. doi: 10.1109/FCS.2018.8597551
20. Wang, D., Zhao, Y., Yi, C., Tsui, K.-L., Lin, J. Sparsity guided empirical wavelet transform for fault diagnosis of rolling element bearings. *Mechanical Systems and Signal Processing*, 2018, Vol 101, pp. 292-308. doi: 10.1016/j.ymssp.2017.08.038
21. Bhattacharyya, A., Singh, L., Pachori, R.B. Fourier-Bessel series expansion based empirical wavelet transform for analysis of non-stationary signals. *Digital Signal Processing*, 2018, Vol. 78, pp. 185-196. doi: 10.1016/j.dsp.2018.02.020